

*A new model of the contact force for the
collision between two solid bodies*

**Hossein Safaeifar & Anooshirvan
Farshidianfar**

Multibody System Dynamics

ISSN 1384-5640

Volume 50

Number 3

Multibody Syst Dyn (2020) 50:233-257

DOI 10.1007/s11044-020-09732-2

Your article is protected by copyright and all rights are held exclusively by Springer Nature B.V.. This e-offprint is for personal use only and shall not be self-archived in electronic repositories. If you wish to self-archive your article, please use the accepted manuscript version for posting on your own website. You may further deposit the accepted manuscript version in any repository, provided it is only made publicly available 12 months after official publication or later and provided acknowledgement is given to the original source of publication and a link is inserted to the published article on Springer's website. The link must be accompanied by the following text: "The final publication is available at link.springer.com".



A new model of the contact force for the collision between two solid bodies

Hossein Safaeifar¹ · Anooshirvan Farshidianfar¹

Received: 1 December 2019 / Accepted: 4 March 2020 / Published online: 1 April 2020
© Springer Nature B.V. 2020

Abstract A collision between two bodies is a usual phenomenon in many engineering applications. The most important problem with the collision analysis is determining the hysteresis damping factor or the hysteresis damping ratio. The hysteresis damping ratio is related to the coefficient of restitution. In this paper, an explicit expression is determined for this relation. For this reason, a parametric expression is considered for the relation between the deformation and its velocity of the contact process. This expression consists of two unknown constants. Using the energy balance, a new explicit parametric expression between the hysteresis damping factor and the coefficient of restitution is derived. For determining the unknown constants, the root mean square (RMS) of the hysteresis damping ratio of this new expression with respect to the numerical model is minimized. This new model is completely suitable for the whole range of the coefficient of restitution. So, the new model can be used in the hard and soft impact problems. Finally, three numerical examples of two colliding bodies, the classic bouncing ball problem, the resilient impact damper, and a planar slider–crank mechanism, are presented and analyzed.

Keywords Collision · Damping · Contact force model · Hysteresis damping factor · Hysteresis damping ratio

Nomenclature

RMS	Root of mean square
F	Contact force
K	Generalized stiffness parameter
Δ	Relative normal deformation
R_1 and R_2	Radii of spheres
σ_1 and σ_2	Material parameters
ν_1 and ν_2	Poisson's ratios

✉ A. Farshidianfar
farshid@um.ac.ir

H. Safaeifar
safaeifar@mail.um.ac.ir

¹ Mechanical Engineering Department, Ferdowsi University of Mashhad, Mashhad, Iran

E_1 and E_2	Young moduli
D	Damping coefficient
C	Hysteresis damping factor
N	Exponent
$\dot{\delta}$	Relative normal velocity of two contacting bodies
c_r	Coefficient of restitution
x_1 and x_2	Displacements of the center of mass
δ_1 and δ_2	Deformations of two spheres
m_1 and m_2	Masses of spheres
\ddot{x}_1 and \ddot{x}_2	Acceleration of the centers of mass of two spheres
m	Equivalent mass
$\ddot{\delta}$	Relative normal acceleration of two contacting bodies
V_1^- and V_2^-	Velocities of the two spheres at the initial instant of contact
V_{12}	Common velocity of both spheres in the maximum deformation instant
$\dot{\delta}^-$ and $\dot{\delta}^+$	Impacting and the separating velocities
ΔT_{com}	Change in the kinetic energy in the compression period
ΔT_{res}	Change in the kinetic energy in the restitution period
ΔT	Total change in the kinetic energy in the contact process
ΔW_{com}	Work done by the Hertz contact force in the compression period
ΔW_{res}	Work done by the Hertz contact force in the restitution period
ΔW	Total work done by the Hertz contact force in the contact process
δ_{max}	Maximum deformation
\ln	Natural logarithm
ΔE_{com}	Energy loss due to the damping force in the compression period
ΔE_{res}	Energy loss due to the damping force in the restitution period
ΔE	Total energy loss due to the damping force in the contact process
h_r	Hysteresis damping ratio
H_0	Initial height of bouncing ball
g	Gravity acceleration
V_0	Initial velocity of bouncing ball

1 Introduction

A collision between two bodies is a usual phenomenon in many engineering applications such as mechanisms [1, 2], robotics [3], biomechanics [4], railway dynamics [5], and impact dampers [6]. The state of mechanical system is changed abruptly in the contact events. The velocities and accelerations of colliding bodies are discontinuous in these problems. This discontinuity causes the nonlinearity of the dynamic behavior of multibody systems. When the two bodies impact each other, the contact force relationship between them must be satisfied. Therefore the contact force model is an important issue in the contact–impact process.

The first work on the collision between two bodies was done by Hertz, who developed the theory now bearing his name [7]. In this theory, a perfectly nonlinear elastic element is considered as the contact force model between the two colliding bodies. The Hertz model is not representing the energy dissipation in the collision process. For this reason, a damping element is added to the Hertz model to account for energy dissipation during the impact of colliding bodies. The combination of the stiffness and the damping element is called the viscoelastic constitutive model. The first viscoelastic impact model is the Kelvin–Voigt

model, which consists of a linear spring and a linear damper element connected in parallel configuration [7]. This model is not very accurate because it does not consider nonlinearity of the impact process. Also the contact force at the beginning of contact is not continuous, because of the existence of the damping element in this model. To solve this problem, Hunt and Crossley proposed a nonlinear viscoelastic model for the contact problems [8].

The most important problem in the nonlinear viscoelastic model is determining the hysteresis damping factor. Many researchers have worked on this matter. Their studies can be divided into four categories. In the first category, the hysteresis damping factor is determined by the experimental tests, as done by Ristow [9], Lee and Herrmann [10], Schäfer et al. [11], Bordbar and Hyppänen [12], as well as Zhang and Sharf [13]. In the second category, an exact equation is proposed for determining the hysteresis damping factor, as done by Herbert and McWhannell [14], Gonthier et al. [15], as well as Zhang and Sharf [16]. The exact equation is a nonlinear function between the hysteresis damping factor and the physical parameters of the contact process. This equation doesn't have an explicit solution, but can be solved numerically. In the third category, a simple assumption is considered and an explicit expression for the hysteresis damping factor is obtained, as done by Hunt and Crossley [8], Lee and Wang [17], Kuwabara and Kono [18], Lankarani and Nikravesh [19], Tsuji et al. [20], Brilliantov et al. [21], Marhefka and Orin [3], as well as Gharib and Hurmuzlu [22]. In the fourth category, the researchers considered an expression for the relation between the deformation and its velocity; an explicit expression between the hysteresis damping factor and the coefficient of restitution was obtained as in Flores et al. [23] and Hu and Guo [24].

Further comparative and review studies of contact force models for solid colliding bodies can be found in [25–30].

In this paper, a new model for contact force between two colliding bodies is derived. For this purpose, the mathematical modeling of a contact process is presented in Sect. 2. The kinetic energy and the work done by the Hertz contact force in the process are obtained in Sects. 3 and 4, respectively. In Sect. 5, the exact expression for the maximum deformation of the contact process is obtained. The energy loss due to the damping force is calculated in Sect. 6. In Sect. 7, the new model for contact force is derived. Finally, three numerical examples of two colliding bodies, the classic bouncing ball problem, the resilient impact damper, and a planar slider–crank mechanism, are presented and analyzed in Sects. 8, 9, and 10, respectively.

2 Mathematical modeling

The Hertz model is the base of most contact force models in the engineering applications. This model relates the contact force and the normal deformation with a nonlinear power function and is expressed as [7, 19, 31, 32]

$$F = K \delta^n \tag{1}$$

where K represents the generalized stiffness parameter and δ is the relative normal deformation between the two contacting bodies. For the two contacting spheres, the generalized parameter K is a function of the radii of the spheres and the material properties. Under this condition, the generalized parameter K can be expressed as [7, 19, 31, 32]

$$K = \frac{4}{3\pi(\sigma_1 + \sigma_2)} \sqrt{\frac{R_1 R_2}{R_1 + R_2}} \tag{2}$$

Table 1 The hysteresis damping factor in some earlier contact force models

The contact force model	The hysteresis damping factor (C)
Hunt and Crossley [8]	$\frac{3(1-c_r)}{2} \frac{K}{\delta^-}$
Lankarani and Nikravesh [19]	$\frac{3(1-c_r^2)}{4} \frac{K}{\delta^-}$
Flores et al. [23]	$\frac{8(1-c_r)}{5c_r} \frac{K}{\delta^-}$
Gharib and Hurmuzlu [22]	$\frac{1}{c_r} \frac{K}{\delta^-}$
Hu and Guo [24]	$\frac{3(1-c_r)}{2c_r} \frac{K}{\delta^-}$

where R_1 and R_2 are the radii of the spheres, and the material parameters of the spheres are given by

$$\sigma_i = \frac{1 - \nu_i^2}{\pi E_i} \quad i = 1, 2 \tag{3}$$

where the variables ν_i and E_i are the Poisson's ratios and the Young moduli of the spheres, respectively. For a contact between sphere 1 and a plane surface of body 2, the generalized stiffness parameter K is expressed as

$$K = \frac{4}{3\pi(\sigma_1 + \sigma_2)} \sqrt{R_1}. \tag{4}$$

It is well known that the Hertz model cannot represent the dissipative energy during the contact process.

Hunt and Crossley presented a nonlinear viscoelastic contact force model which can be expressed as [8]

$$F = K \delta^n + D \dot{\delta} \tag{5}$$

where the exponent n is usually set to 3/2 in the Hertz model [19]. Hunt and Crossley proposed that the damping coefficient D be expressed as [8]

$$D = C \delta^n \tag{6}$$

where C is the hysteresis damping factor. So the contact force between the two colliding spheres is expressed as

$$F = K \delta^{3/2} + C \delta^{3/2} \dot{\delta}. \tag{7}$$

The relations between the hysteresis damping factor and the coefficient of restitution in some earlier contact force models are listed in Table 1.

Each contact process consists of two phases. The first is named compression, the approaching or loading period, while the other is restitution, the separating or unloading period [7]. The two spheres come in contact and reach their maximum deformation during the compression period. In this period, the deformation velocity is reduced from its initial value to zero. The two spheres separate from each other during the restitution period, in which the deformation velocity is increased to its maximum value.

Figure 1 shows the contact between the two spheres. In this figure, x_1 , x_2 , δ_1 and δ_2 represent the displacements of the center of mass and the deformations of both spheres, respectively, just like the parameters m_1 , m_2 , R_1 , and R_2 that represent the masses and the radii of both spheres.

Fig. 1 The contact between two spheres

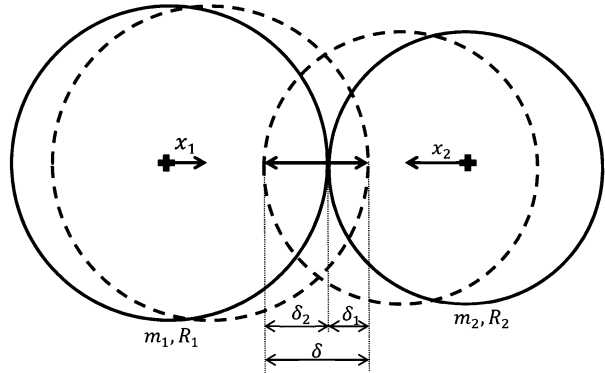
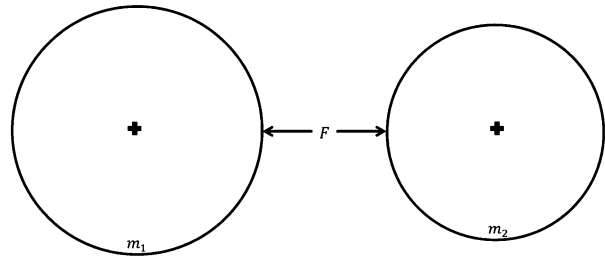


Fig. 2 Free diagrams of two spheres



In Fig. 1, the total deformation δ is the sum of both spheres, i.e., $\delta = \delta_1 + \delta_2$. The total deformation is also equal to the relative motion between the two spheres and can be expressed as [33]

$$\delta = x_1 + x_2. \tag{8}$$

It is be noted that the deformation of each sphere in not equal to the displacement of the center of mass, i.e., $\delta_1 \neq x_1$ and $\delta_2 \neq x_2$.

The free diagram of two spheres in contact is shown in Fig. 2. In this figure, F represents the contact force between the two colliding spheres and expressed by (7).

Using the Newton's second law, the acceleration of the center of mass of each sphere can be obtained as:

$$\ddot{x}_1 = -\frac{F}{m_1}, \tag{9}$$

$$\ddot{x}_2 = -\frac{F}{m_2}. \tag{10}$$

By double differentiation of (8) and combining with (9) and (10), the mathematical representation of the dynamical equivalent system can be expressed as

$$m\ddot{\delta} + F = 0 \tag{11}$$

where $\ddot{\delta}$ represents the acceleration of the equivalent system and the equivalent mass, m , is given by

$$m = \frac{m_1 m_2}{m_1 + m_2}. \tag{12}$$

Using (7) and (11), the mathematical model of the dynamical system can be expressed as

$$m\ddot{\delta} + C\delta^{3/2}\dot{\delta} + K\delta^{3/2} = 0. \tag{13}$$

The mathematical model (13) is a second-order ordinary differential equation with variable coefficients. This equation doesn't have an analytical solution.

3 The kinetic energy

The balance of the linear momentum for the two spheres between the initial instant and the maximum deformation instant of the contact can be expressed as [34]

$$m_1 V_1^- + m_2 V_2^- = (m_1 + m_2) V_{12} \tag{14}$$

where V_1^- and V_2^- are velocities of the two spheres in the initial instant of contact. So, the common velocity of both spheres in the maximum deformation instant of the contact can be obtained as

$$V_{12} = \frac{m_1 V_1^- + m_2 V_2^-}{m_1 + m_2}. \tag{15}$$

The coefficient of restitution is defined as the ratio between the deformation velocity at the separation and the deformation velocity at the initial contact of the two spheres and can be expressed as

$$c_r = -\frac{\dot{\delta}^+}{\dot{\delta}^-} \tag{16}$$

where $\dot{\delta}^-$ and $\dot{\delta}^+$ represent the impacting and the separating velocities, respectively.

The change in the kinetic energy in the compression period of the contact process can be expressed as

$$\Delta T_{\text{com}} = \frac{1}{2}(m_1 + m_2)V_{12}^2 - \left(\frac{1}{2}m_1(V_1^-)^2 + \frac{1}{2}m_2(V_2^-)^2 \right). \tag{17}$$

Using $V_1^- = \dot{\delta}_1^-$, $V_2^- = -\dot{\delta}_2^-$, $\dot{\delta}^- = \dot{\delta}_1^- + \dot{\delta}_2^-$ and combining with (15), (16), and (17), the change in the kinetic energy in the compression period is obtained as

$$\Delta T_{\text{com}} = -\frac{1}{2}m(\dot{\delta}^-)^2 \tag{18}$$

where m is the equivalent mass as given by (12).

Similarly, the change in the kinetic energy in the restitution period can be expressed as

$$\Delta T_{\text{res}} = +\frac{1}{2}m(\dot{\delta}^+)^2. \tag{19}$$

The total change in the kinetic energy in the contact process of the two solid spheres is the sum of the changes in the kinetic energy in the compression and the restitution periods. The total change in the kinetic energy can be obtained as

$$\Delta T = -\frac{1}{2}m(\dot{\delta}^-)^2(1 - c_r^2). \tag{20}$$

Equation (20) represents the kinetic energy loss in the contact process of the two solid spheres in terms of the initial deformation velocity and the coefficient of restitution. For a fully elastic contact, the coefficient of restitution is equal to one, so the change in the kinetic energy in this contact is zero. For a fully plastic contact, the coefficient of restitution is null, so the change in the kinetic energy in this contact is maximized.

4 The work done by the Hertz contact force

The work done by the Hertz contact force in the compression period of the contact process can be expressed as

$$\Delta W_{\text{com}} = \int_0^{\delta_{\text{max}}} (-K \delta^{3/2}) d\delta \tag{21}$$

which can be obtained as

$$\Delta W_{\text{com}} = -\frac{2}{5} K \delta_{\text{max}}^{5/2}. \tag{22}$$

Similarly, the work done by the Hertz contact force in the restitution period can be obtained as

$$\Delta W_{\text{res}} = \frac{2}{5} K \delta_{\text{max}}^{5/2}. \tag{23}$$

So, the total work done by the Hertz contact force in the contact process can be obtained as

$$\Delta W = \Delta W_{\text{com}} + \Delta W_{\text{res}} = 0. \tag{24}$$

5 The maximum deformation

The relation between the deformation and its velocity can be expressed as [34]

$$\dot{\delta} d\dot{\delta} = \ddot{\delta} d\delta. \tag{25}$$

This equation is a relation between distance, velocity, and acceleration in 1 DOF motion of a particle.

Using (13), the acceleration of the equivalent 1-DOF system can be obtained as

$$\ddot{\delta} = -\frac{C \delta^{3/2} \dot{\delta} + K \delta^{3/2}}{m}. \tag{26}$$

Combining (25) and (26) gives

$$\dot{\delta} d\dot{\delta} = -\frac{C \delta^{3/2} \dot{\delta} + K \delta^{3/2}}{m} d\delta. \tag{27}$$

Equation (27) can be represented as

$$\frac{\dot{\delta}}{K + C \dot{\delta}} d\dot{\delta} = -\frac{\delta^{3/2}}{m} d\delta. \tag{28}$$

Integrating (28) from $\dot{\delta}^-$ to 0 for $\dot{\delta}$ and from 0 to δ_{\max} for δ , the maximum deformation of the contact process can be obtained as

$$\delta_{\max} = \left(\frac{5m}{2C} \left(\dot{\delta}^- - \frac{K}{C} \ln \left(\frac{K + C\dot{\delta}^-}{K} \right) \right) \right)^{2/5}. \tag{29}$$

Equation (29) is an exact expression for the maximum deformation of the contact process.

6 The energy loss due to the damping force

The energy loss due to the damping force in the compression period can be expressed as

$$\Delta E_{\text{com}} = \int_0^{\delta_{\max}} (-C\delta^{3/2}\dot{\delta})d\delta. \tag{30}$$

This energy is dissipated in the thermal form and the plastic deformation in the colliding bodies.

For evaluation of Eq. (30), the relation between the deformation and its velocity must be specified.

Integrating (28) from $\dot{\delta}^-$ to $\dot{\delta}_{\text{com}}$ for $\dot{\delta}$ and from 0 to δ_{com} for δ , the relation between the deformation and its velocity in the compression period can be obtained as

$$\delta_{\text{com}} = \left(\frac{5m}{2C} \left((\dot{\delta}^- - \dot{\delta}_{\text{com}}) - \frac{K}{C} \ln \left(\frac{K + C\dot{\delta}^-}{K + C\dot{\delta}_{\text{com}}} \right) \right) \right)^{2/5}. \tag{31}$$

Combining (31) with (30), the energy loss due to the damping force in the compression period can be obtained as

$$\Delta E_{\text{com}} = m \left(\frac{-(\dot{\delta}^-)^2}{2} + \frac{K}{C}\dot{\delta}^- + \left(\frac{K}{C} \right)^2 \ln \left(\frac{K}{K + C\dot{\delta}^-} \right) \right). \tag{32}$$

Similarly, the energy loss due to the damping force in the restitution period can be obtained as

$$\Delta E_{\text{res}} = m \left(\frac{(\dot{\delta}^+)^2}{2} - \frac{K}{C}\dot{\delta}^+ + \left(\frac{K}{C} \right)^2 \ln \left(\frac{K + C\dot{\delta}^+}{K} \right) \right). \tag{33}$$

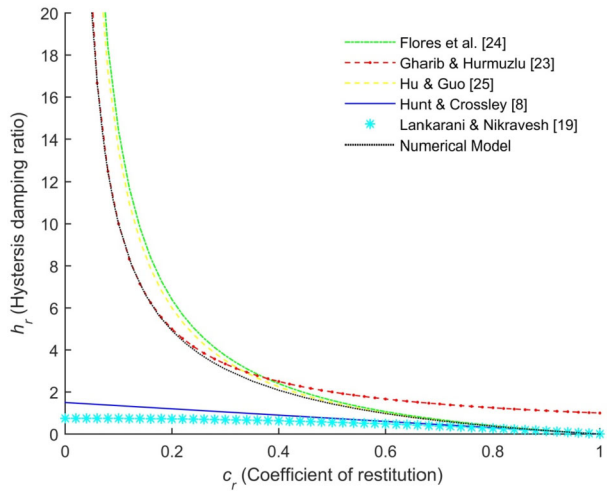
The total energy loss due to the damping force in the contact process of the two solid spheres is the sum of the energy losses in the compression and the restitution periods. So, the total energy loss due to the damping force can be calculated as

$$\begin{aligned} \Delta E = & -\frac{1}{2}((\dot{\delta}^-)^2 - (\dot{\delta}^+)^2) + \frac{mK}{C}(\dot{\delta}^- - \dot{\delta}^+) \\ & + m \left(\frac{K}{C} \right)^2 \left(\ln \left(\frac{K}{K + C\dot{\delta}^-} \right) + \ln \left(\frac{K + C\dot{\delta}^+}{K} \right) \right). \end{aligned} \tag{34}$$

Combining (16) and (34) gives

$$\Delta E = -\frac{1}{2}(\dot{\delta}^-)^2(1 - c_r^2) + \frac{mK}{C}\dot{\delta}^-(1 + c_r) + m \left(\frac{K}{C} \right)^2 \ln \left(\frac{K - Cc_r\dot{\delta}^-}{K + C\dot{\delta}^-} \right). \tag{35}$$

Fig. 3 The hysteresis damping ratio versus the coefficient of restitution in the numerical model and earlier models



The balance of the energy in the contact process can be expressed as

$$\Delta W + \Delta E = \Delta T. \tag{36}$$

Combining (20), (24), and (35) with (36) gives

$$\dot{\delta}^-(1 + c_r) + \frac{K}{C} \ln\left(\frac{K - Cc_r\dot{\delta}^-}{K + C\dot{\delta}^-}\right) = 0. \tag{37}$$

For simplicity, the hysteresis damping ratio is defined as

$$h_r = \frac{C\dot{\delta}^-}{K}. \tag{38}$$

So, the relation between the hysteresis damping ratio and the coefficient of restitution can be expressed as

$$h_r(1 + c_r) = \ln\left(\frac{1 + h_r}{1 - c_r h_r}\right). \tag{39}$$

This relation is the exact equation between the hysteresis damping ratio and the coefficient of restitution as obtained by Zhang and Sharf [16]. This equation has no explicit solution, but can be solved numerically. In this paper, this numerical solution is called the numerical model. To derive an explicit expression for the relation between the hysteresis damping ratio and the coefficient of restitution, a simpler relation between the deformation and its velocity can be considered instead of (31).

The relation between the hysteresis damping ratio and the coefficient of restitution in the numerical model and the earlier models are shown in Fig. 3.

All the models presented in Fig. 3, except the Gharib and Hurmuzlu model [22], have a similar response when the value of the coefficient of restitution is higher than 0.8. The contact force approaches by Flores et al. [23], Gharib and Hurmuzlu [22], Hu and Guo [24], and the numerical model have a similar behavior for moderate and low values of the coefficient of restitution. Indeed, when the coefficient of restitution is equal to zero, the hysteresis

damping ratio and the hysteresis damping factor in these models become infinite, which is logical from the physical view of the contact process.

The numerical model is nearly equivalent to the real contact force model. So for the low values of coefficient of restitution, Gharib and Hurmuzlu model is closer to reality but this model is originally not proper for the high values of coefficient of restitution. For such values, Flores et al. and Hu and Guo models are closer to reality.

It can be observed that the behavior of Flores et al. [23] and Hu and Guo [24] models is very similar to the numerical model in the whole range of the coefficient of restitution.

Flores et al. used the solution of the Kelvin–Voigt model and considered the relation between the deformation and its velocity as [23]

$$\frac{\dot{\delta}}{\dot{\delta}^-} = \left(1 - \left(\frac{\delta}{\delta_{\max}} \right)^2 \right)^{\frac{1}{2}}. \tag{40}$$

Hu and Guo used the solution of the Hertz model and considered the relation between the deformation and its velocity as [24]

$$\frac{\dot{\delta}}{\dot{\delta}^-} = \left(1 - \left(\frac{\delta}{\delta_{\max}} \right)^{\frac{5}{2}} \right)^{\frac{1}{2}}. \tag{41}$$

Similarly, in this paper, a parametric expression is considered for the relation between the deformation and its velocity in the compression period given by

$$\frac{\dot{\delta}}{\dot{\delta}^-} = \left(1 - \left(\frac{\delta}{\delta_{\max}} \right)^a \right)^{\frac{1}{b}} \tag{42}$$

where a and b are two unknown constants.

Combining (30) and (42) gives

$$\Delta E_{\text{com}} = \int_0^{\delta_{\max}} \left(-C\delta^{3/2}\dot{\delta}^- \left(1 - \left(\frac{\delta}{\delta_{\max}} \right)^a \right)^{\frac{1}{b}} \right) d\delta. \tag{43}$$

Considering $\delta/\delta_{\max} = y$ gives

$$\Delta E_{\text{com}} = -C\delta_{\max}^{5/2}\dot{\delta}^- \int_0^1 y^{3/2}(1 - y^a)^{\frac{1}{b}} dy. \tag{44}$$

Introducing $I = \int_0^1 y^{3/2}(1 - y^a)^{\frac{1}{b}} dy$ gives

$$\Delta E_{\text{com}} = -IC\delta_{\max}^{5/2}\dot{\delta}^-. \tag{45}$$

Similarly, the energy loss due to the damping force in the restitution period can be obtained as

$$\Delta E_{\text{res}} = IC\delta_{\max}^{5/2}\dot{\delta}^+. \tag{46}$$

So, the total energy loss due to the damping force in the contact process of two solid spheres can be calculated as

$$\Delta E = -IC\delta_{\max}^{5/2}(\dot{\delta}^- - \dot{\delta}^+). \tag{47}$$

Combining (16) with (47) gives

$$\Delta E = -IC\delta_{\max}^{5/2}\dot{\delta}^- (1 + c_r). \tag{48}$$

As shown in (28), the relation between the deformation and the deformation velocity is related to K , C , and m . Using (2), (3), and (12), it is clear that the relation between the deformation and deformation velocity is related to the modulus of elasticity, Poisson's ratio, radius, and mass of two colliding bodies. Equation (42) show a combination of parameters a and b that determine the relation between the deformation and the deformation velocity. An integral combination of these two parameters is equal to parameter I . So parameters a , b and I are related to the modulus of elasticity, Poisson's ratio, radius, and mass of two colliding bodies.

7 The new contact force model

The energy balance in the compression period of the contact process can be expressed as [34]

$$\Delta E_{\text{com}} + \Delta W_{\text{com}} = \Delta T_{\text{com}}. \tag{49}$$

Combining (18), (22), and (46) with (49) gives

$$-IC\delta_{\max}^{5/2}\dot{\delta}^- - \frac{2}{5}K\delta_{\max}^{5/2} = -\frac{1}{2}m(\dot{\delta}^-)^2. \tag{50}$$

Solving Eq. (50) gives

$$\delta_{\max}^{5/2} = \frac{\frac{1}{2}m(\dot{\delta}^-)^2}{\frac{2}{5}K + IC\dot{\delta}^-}. \tag{51}$$

So, the maximum deformation in the contact process can be obtained by

$$\delta_{\max} = \left(\frac{\frac{1}{2}m(\dot{\delta}^-)^2}{\frac{2}{5}K + IC\dot{\delta}^-} \right)^{2/5}. \tag{52}$$

Combining (20), (24), (48), and (51) with (36) gives

$$-IC\left(\frac{\frac{1}{2}m(\dot{\delta}^-)^2}{\frac{2}{5}K + IC\dot{\delta}^-} \right)\dot{\delta}^- (1 + c_r) + 0 = -\frac{1}{2}m(\dot{\delta}^-)^2(1 - c_r^2). \tag{53}$$

Solving (53), the hysteresis damping factor can be obtained as

$$C = \frac{2}{5I} \frac{(1 - c_r)}{c_r} \frac{K}{\dot{\delta}^-}. \tag{54}$$

So, the hysteresis damping ratio in the new model can be expressed as

$$h_r = \frac{2}{5I} \frac{(1 - c_r)}{c_r} \tag{55}$$

where I is a function of two unknown constants a and b . To determine a and b , the RMS of the percentage error of the hysteresis damping ratio of the new model with respect to the

Table 2 The RMS of the percentage error of the hysteresis damping ratio of the new model with respect to the numerical model

<i>a</i>	<i>b</i>									
	1.5	2	2.5	3	3.5	4	4.5	5	5.5	6
1	95.092	61.628	43.599	32.598	25.416	20.575	17.303	15.144	13.794	13.030
1.5	62.251	40.756	28.937	21.838	17.468	14.853	13.417	12.761	12.596	12.718
2	44.786	29.438	21.136	16.483	14.015	12.904	12.597	12.729	13.078	13.521
2.5	34.047	22.566	16.708	13.873	12.774	12.612	12.901	13.379	13.917	14.455
3	26.921	18.221	14.266	12.812	12.620	12.983	13.549	14.161	14.756	15.308
3.5	22.003	15.496	13.067	12.599	12.949	13.576	14.257	14.910	15.508	16.046
4	18.564	13.875	12.632	12.813	13.464	14.212	14.932	15.584	16.164	16.676
4.5	16.178	13.010	12.640	13.221	14.027	14.824	15.544	16.178	16.732	17.217
5	14.572	12.649	12.886	13.701	14.581	15.387	16.091	16.700	17.226	17.683
5.5	13.547	12.609	13.250	14.196	15.103	15.897	16.578	17.159	17.657	18.088
6	12.953	12.763	13.663	14.676	15.584	16.357	17.010	17.564	18.036	18.442

numerical model is minimized. The RMS of the percentage error of the hysteresis damping ratio of the new model with respect to the numerical model for various values of *a* and *b* is listed in Table 2.

It is clear that the RMS of the percentage error is minimized at *a* = 1.5 and *b* = 5.5. This minimized value is 12.596. So, the relation between the deformation and its velocity can be expressed as

$$\frac{\dot{\delta}}{\delta^-} = \left(1 - \left(\frac{\delta}{\delta_{\max}} \right)^{\frac{3}{2}} \right)^{\frac{2}{11}} \tag{56}$$

Thus, parameter *I* can be expressed as

$$I = \int_0^1 (y^{3/2} (1 - y^{3/2})^{2/11}) dy \tag{57}$$

which can be evaluated as

$$I = 0.3180 \approx 0.3200 = \frac{8}{25} \tag{58}$$

It is being noted that the RMS of the percentage error of Flores et al. and Hu and Guo models is 29.438 and 22.566, respectively. These values are much greater than the RMS of the minimized value, which is 12.596.

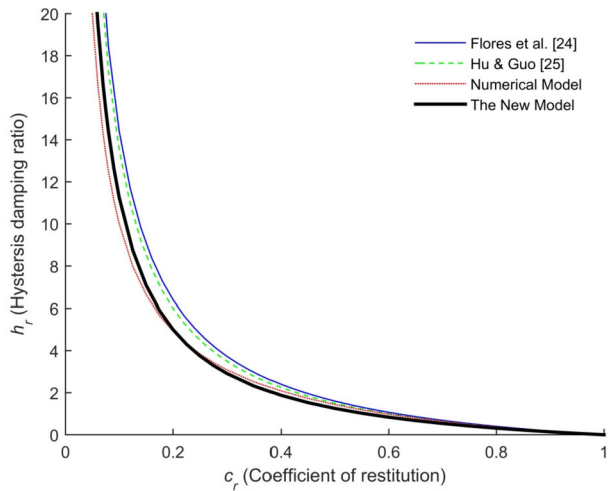
Combining (55) with (58), the hysteresis damping ratio can be obtained as

$$h_r = \frac{5}{4} \frac{(1 - c_r)}{c_r} \tag{59}$$

The relation (59) is called the new model. The relation between the hysteresis damping ratio and the coefficient of restitution in the new model, the numerical model, as well as Flores et al. [23] and Hue and Guo [24] models are shown in Fig. 4.

Although Flores et al. and Hu and Guo models have similar behavior as the numerical model, they are not completely consistent with the numerical model for the low values of the coefficient of restitution.

Fig. 4 The hysteresis damping ratio versus the coefficient of restitution in the contact force models



Analyzing Fig. 4, it is clear that the new model is completely consistent with the numerical model in the whole range of the coefficient of restitution. So, the new model can be selected as the best contact force model for the collision between the two solid spheres in the whole range of the coefficient of restitution. Thus, this new model can be used in the hard and soft impact problems.

The same result can be obtained by another way. The contact force model is performed by using the input coefficient of restitution ($c_{r,in}$). Then the deformation velocity at separation time (δ^+) is obtained by using the new contact force model. Thus, the output coefficient of restitution is obtained as

$$c_{r,out} = -\frac{\delta^+}{\delta^-}. \tag{60}$$

It can be found that the output coefficient of restitution differs from the input coefficient of restitution, but they should be the same value theoretically. The plots of the output coefficient of restitution versus the input coefficient of restitution for different contact force models are shown in Fig. 5. The error of the output coefficient of restitution with respect to the input coefficient of restitution for various contact force models are plotted in Fig. 6.

Analyzing Figs. 5 and 6 shows that the error of the new model for low values of the coefficient of restitution (e.g., less than 0.4) is less than the error of Flores et al. and Hu and Guo models. So the new model is closer to reality for low values of the coefficient of restitution.

Analyzing Figs. 3, 4, 5, and 6 shows that the contact force models can be divided into four groups. In the first group, the contact force models are suitable for the high values of the coefficient of restitution. All of the models, except for Gharib and Hurmuzlu model, are placed in this group. In the second group, the contact force models are suitable for the low and moderate values of the coefficient of restitution, such as Flores et al. model, Gharib and Hurmuzlu model, Hu and Guo model, and the new model derived in this paper. In the third group, the contact force models are nearly suitable for the whole range of the coefficient of restitution and include Flores et al. and Hu and Guo models. In the fourth group, the contact force models are completely suitable for the whole range of the coefficient of restitution. The new model is placed in this group.

Fig. 5 The relation between the output and the input coefficients of restitution

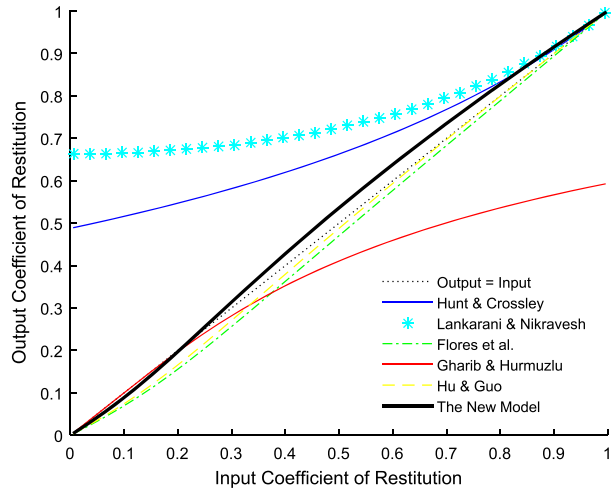
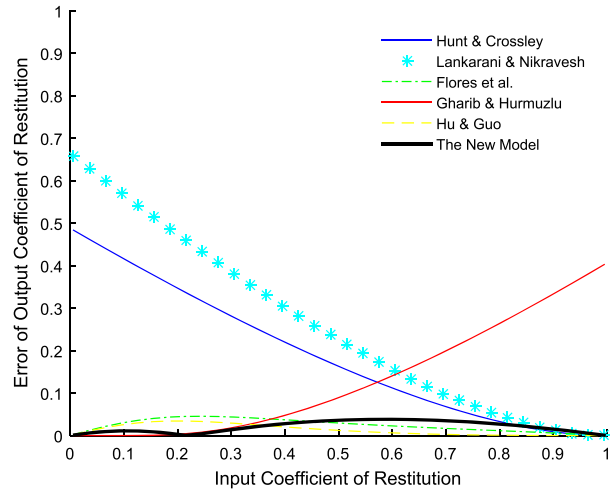


Fig. 6 The error of output coefficients of restitutions respect to the input coefficients of restitution



The hysteresis damping factor in the new model can be obtained as

$$C = \frac{5(1 - c_r) K}{4 c_r \dot{\delta}^-} \tag{61}$$

Thus, the new model of the contact force can be expressed as

$$F = K \delta^{3/2} \left(1 + \frac{5(1 - c_r) \dot{\delta}}{4 c_r \dot{\delta}^-} \right) \tag{62}$$

It is important to point out that the new model is valid for the direct central and frictionless impacts. In perfectly elastic contacts when the coefficient of restitution is equal to one, the hysteresis damping factor is zero and the new model is equivalent to the Hertz model. When the coefficient of restitution is equal to zero, the hysteresis damping factor become infinite, which is logical from the physical view of the contact process.

Fig. 7 The bouncing ball

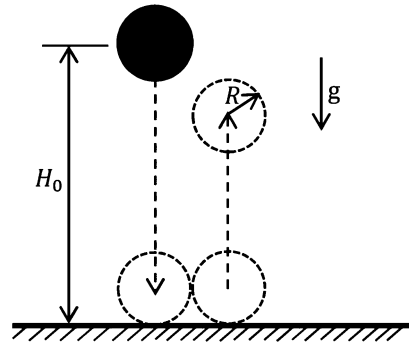


Fig. 8 The contact force versus the deformation for $c_r = 0.2$

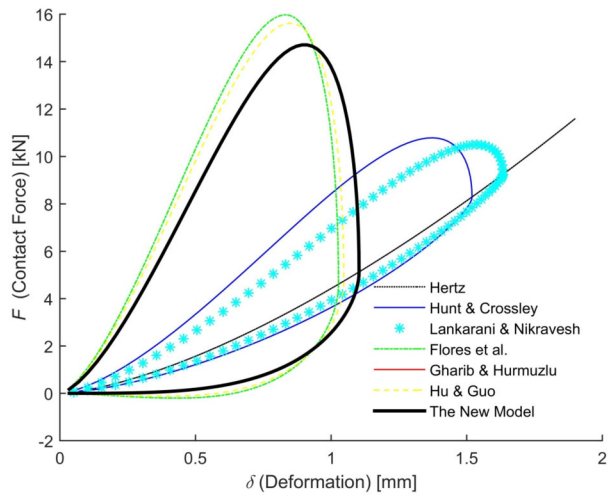


Table 3 Numerical values for the bouncing ball problem [24]

Parameter	Value
Mass	$m = 1.0 \text{ kg}$
Radius	$R = 0.1 \text{ m}$
Initial height	$H_0 = 1.0 \text{ m}$
Gravity acceleration	$g = 9.8 \text{ m/s}^2$
Equivalent stiffness	$K = 1.4 \times 10^8 \text{ N/m}^{3/2}$
Initial velocity	$V_0 = 0 \text{ m/s}$

8 Example 1: the bouncing ball problem

A numerical example, the classic bouncing problem, which is a simple example for analyzing the contact process, is considered here to compare the new model with the earlier contact force models listed in Table 1. The model of this problem is shown in Fig. 7. The numerical values of this example are listed in Table 3 [24].

The bouncing ball falls down and collides with the ground. The ground is assumed to be rigid and stationary. The initial velocity of the ball when it collides with the ground can be

Fig. 9 The contact force versus the deformation for $c_r = 0.4$

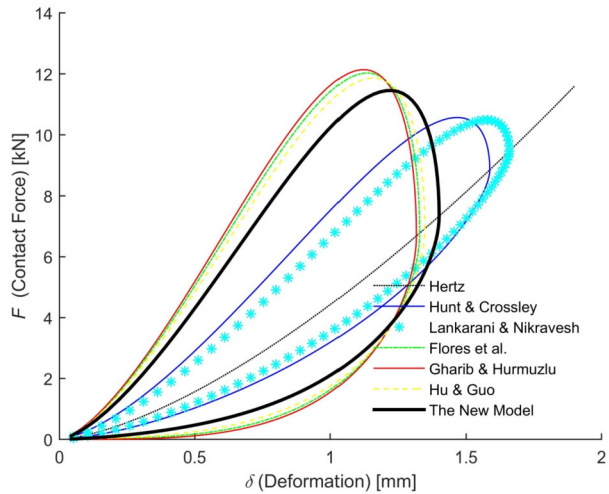
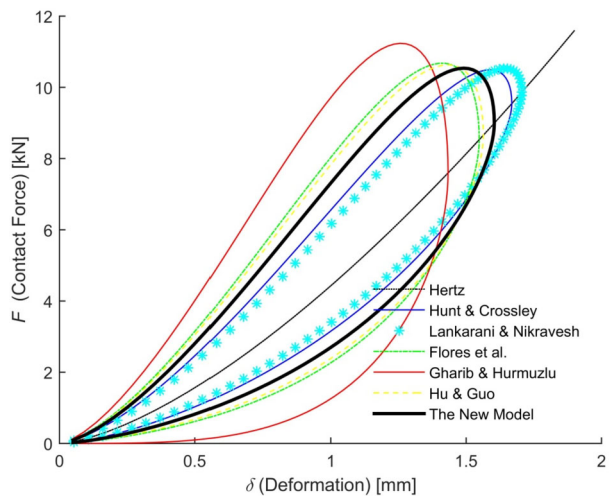


Fig. 10 The contact force versus the deformation for $c_r = 0.6$



expressed as [34]

$$\delta^- = \sqrt{2g(H_0 - R)} \tag{63}$$

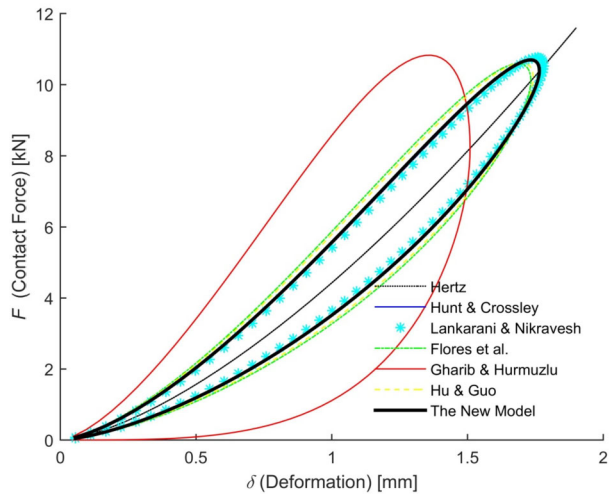
where g represents gravity acceleration. In relation (63), H_0 and R are the initial height of the center of mass and the radius of the ball, respectively.

The new model, the Hertz model, and the earlier contact force models are used to calculate the contact force, deformation, and time of the contact during the contact process between the ball and the ground. Analyzing this problem is done by using Matlab codes. The contact force versus the deformation for four values of the coefficient of restitution (0.2, 0.4, 0.6, and 0.8) is plotted in Figs. 8, 9, 10, and 11, respectively.

By analyzing Figs. 8–11, the following results are obtained:

1. When the coefficient of restitution is high, i.e., 0.8, all of the models, except for Gharib and Hurmuzlu model, have a similar behavior and become very similar to Hertz model.

Fig. 11 The contact force versus the deformation for $c_r = 0.8$



2. When the coefficient of restitution is low, i.e., 0.2, Flores et al. model, Gharib and Hurmuzlu model, Hu and Guo model, and the new model have a similar behavior.
3. When the coefficient of restitution is increasing (from Fig. 8 to Fig. 11), the maximum deformation increases while the maximum contact force is reduced. These results are expected because of decreasing in energy loss due to damping force while the coefficient of restitution is increasing.

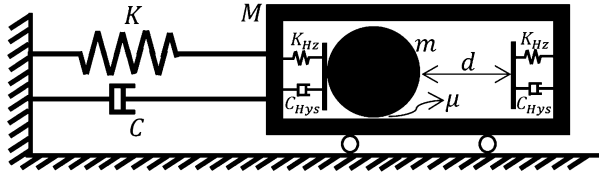
9 Example 2: the resilient impact damper

The impact damper is a passive device composed of one or more cavities that are filled with dry granular particles such as granules of steel, aluminum, lead, tungsten carbide, or ceramic [35]. The impact damper consists of one or several small masses which are mounted on top or inside the vibrating system. When the primary system vibrates, the impact mass moves and collides with fixed stops of the mounting system. These collisions lead to the momentum transfer from the primary system to the impact mass. The kinetic energy of the vibrating system equipped with the impact damper gets dissipated due to impact between impact and primary masses, friction and sound radiation. So the kinetic energy of the primary system is reduced and the vibrating motion gets damped.

The impact dampers can be classified into rigid and resilient. For low contact velocity and high modulus of elasticity, the impact damper can be considered as rigid. While for high contact velocity and low modulus of elasticity, the impact damper is resilient. In the rigid impact damper, the contact time is very small. Thus the changes in the positions of the primary and impact masses can be neglected. So the positions after contact can be considered equal to those before contact. In the resilient impact damper, the contact time is not negligible. So the changes in the positions of the primary and impact masses must be considered.

Figure 12 shows a schematic of a 1-DOF system equipped with the resilient single-unit impact damper.

Fig. 12 The 1-DOF system equipped with resilient impact damper



When there is no contact between the impact and primary masses, the equations of motion of the system can be written as

$$\begin{aligned}
 -C\dot{x}_M - Kx_M - \mu mg \operatorname{sgn}(\dot{x}_M - \dot{x}_m) &= M\ddot{x}_M \\
 \mu mg \operatorname{sgn}(\dot{x}_M - \dot{x}_m) &= m\ddot{x}_m
 \end{aligned}
 \tag{64}$$

where x_M and x_m are the positions of the primary and the impact masses, respectively; μ is the kinetic friction coefficient between these two masses. Dot and double dot denote the first and second derivatives with respect to time, respectively. These equations are a system of two nonhomogeneous coupled second-order ordinary differential equations with constant coefficients and so can be solved analytically as

$$\begin{aligned}
 x_M(t) &= e^{-\xi\omega_n t} \{A \sin(\sqrt{1 - \xi^2}t) + B \cos(\sqrt{1 - \xi^2}t)\} - \mu \frac{m}{K} g \operatorname{sgn}(\dot{x}_M - \dot{x}_m), \\
 x_m(t) &= \frac{1}{2} \mu g \operatorname{sgn}(\dot{x}_M - \dot{x}_m) t^2 + Ct + D
 \end{aligned}
 \tag{65}$$

where ω_n , ξ , and t represent the natural frequency, damping ratio, and time, respectively. The initial conditions are considered parametrically as

$$\begin{aligned}
 x_M(t_0) &= x_{M,0}, & \dot{x}_M(t_0) &= V_{M,0}, \\
 x_m(t_0) &= x_{m,0}, & \dot{x}_m(t_0) &= V_{m,0}.
 \end{aligned}
 \tag{66}$$

Using these initial conditions, the general solution of the equations of motion can be determined. The contact situation between main mass and impact mass can be determined using the following relations:

$$\begin{aligned}
 x_m - (x_M - d/2) &= 0 & (\text{Contact between impact mass and left side}), \\
 (x_M + d/2) - x_m &= 0 & (\text{Contact between impact mass and right side})
 \end{aligned}
 \tag{67}$$

where d is the gap size.

When contact occurs between impact mass and two end stoppers, the contact force between them must be added to the equations of motion. In this situation, the equations of motions can be written as

$$\begin{aligned}
 M\ddot{x}_M + C\dot{x}_M + Kx_M + \mu mg \operatorname{sgn}(\dot{x}_M - \dot{x}_m) + F_{\text{contact}} &= 0 \\
 m\ddot{x}_m - \mu mg \operatorname{sgn}(\dot{x}_M - \dot{x}_m) - F_{\text{contact}} &= 0
 \end{aligned}
 \tag{68}$$

where F_{contact} is the contact force between the impact and main masses. By defining the deformation between impact mass and the left side of main mass container as $\delta = (x_M - d/2) - x_m$ and also using the new contact force model described in this article, the equations

Fig. 13 Time response of impact mass and left and right sides of the container (the impact damper with 10 mm gap size)

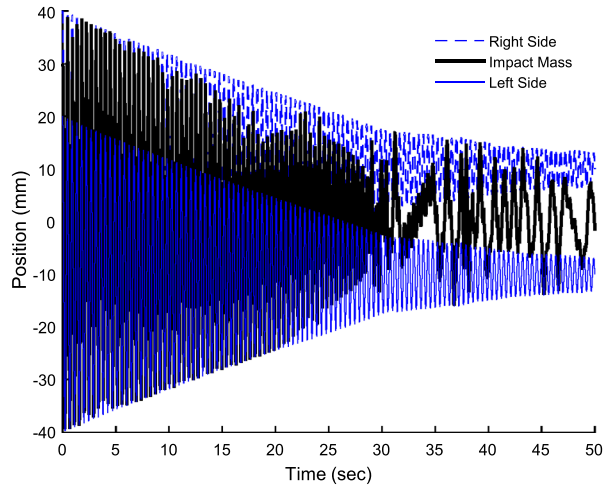


Table 4 Numerical values for the impact damper problem

Parameter	Value
Main mass	$M = 500$ gr
Impact mass	$m = 4$ gr
Stiffness of main mass	$K = 100$ N/m
Damping ratio of main mass	$\xi = 0.003$
Generalized stiffness	$K_{Hz} = 1 \times 10^8$ N/m ^{3/2}
Coefficient of restitution	$c_r = 0.7$
Coefficient of kinetic friction	$\mu = 0.1$
Initial displacement of main mass	$x_0 = 0.03$ m
Initial velocity of main mass	$V_0 = 0$ m/s

of motion can be obtained as

$$\begin{aligned}
 &M\ddot{x}_M + C\dot{x}_M + Kx_M + \mu mg \operatorname{sgn}(\dot{x}_M - \dot{x}_m) \\
 &\quad + K_{Hz}(x_M - d/2) - x_m)^{\frac{3}{2}} \left(1 + \frac{5}{4} \frac{1 - c_r}{c_r \dot{\delta}^-} (\dot{x}_M - \dot{x}_m)\right) = 0 \\
 &m\ddot{x}_m - \mu mg \operatorname{sgn}(\dot{x}_M - \dot{x}_m) \\
 &\quad - K_{Hz}(x_M - d/2) - x_m)^{\frac{3}{2}} \left(1 + \frac{5}{4} \frac{1 - c_r}{c_r \dot{\delta}^-} (\dot{x}_M - \dot{x}_m)\right) = 0
 \end{aligned} \tag{69}$$

where K_{Hz} is the generalized stiffness parameter which can be determined using Eq. (2) or (4). These equations form a system of two coupled nonlinear differential equations. They cannot be solved analytically but can be solved numerically.

The numerical values of this example are listed in Table 4.

Figure 13 shows the time response of the positions of the impact mass and two end stoppers in the impact damper with 20 mm gap size. As shown in this figure, the behavior of this damper can be classified into three zones. In the first zone, from 0 to 30 seconds, the impact mass has effective collisions with two end stoppers. This zone is named the impact

Fig. 14 Amplitude of position of 1-DOF system equipped with impact damper with 20 mm gap size

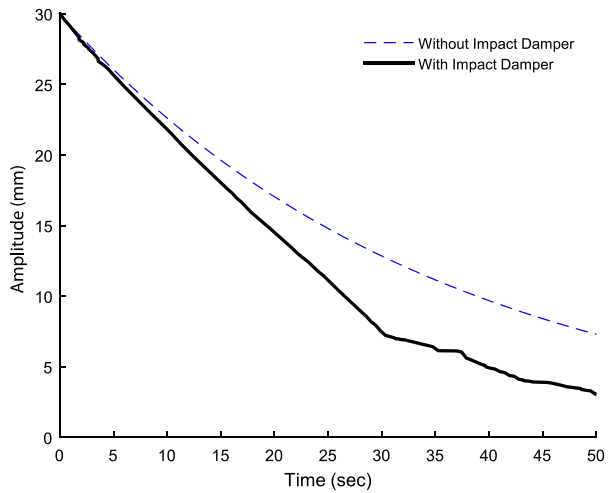
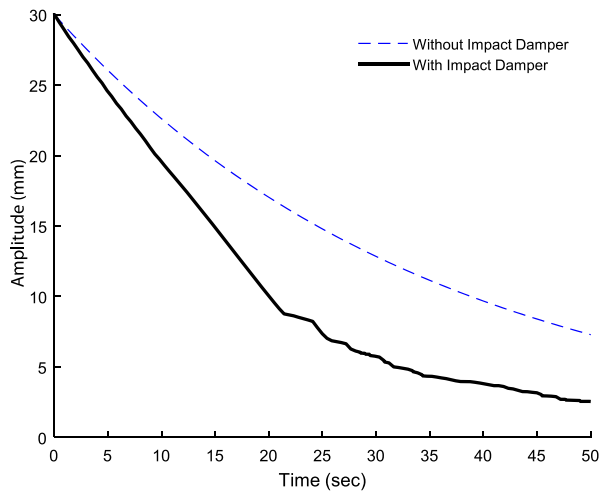


Fig. 15 Amplitude of position of 1-DOF system equipped with impact damper with 30 mm gap size



zone. The effect of friction and structural damping is insignificant in the impact zone. In this zone, the decreasing rate of the amplitude of the position of the primary mass is nearly linear. In the second zone, from 30 to 45 seconds, the collisions between the impact mass and two end stoppers is not so effective. The reason for the movement of the impact mass in this zone is mainly the friction between the impact mass and the guiding bars. This zone is named the friction zone. In the third zone, after 45 seconds, the movement of impact mass relative to the end stoppers is nearly insignificant. In this zone, the dynamic behavior of this system is similar to the behavior of the system without an impact damper. This zone is named the no-impact zone.

For simplifying response graphs, the amplitude of the position of the 1-DOF system can be displayed. Figures 14, 15, 16 and 17 show the amplitude of the position response in the 1-DOF system equipped with an impact damper with 20, 30, 40, and 50 mm gap size, respectively.

Fig. 16 Amplitude of position of 1-DOF system equipped with impact damper with 40 mm gap size

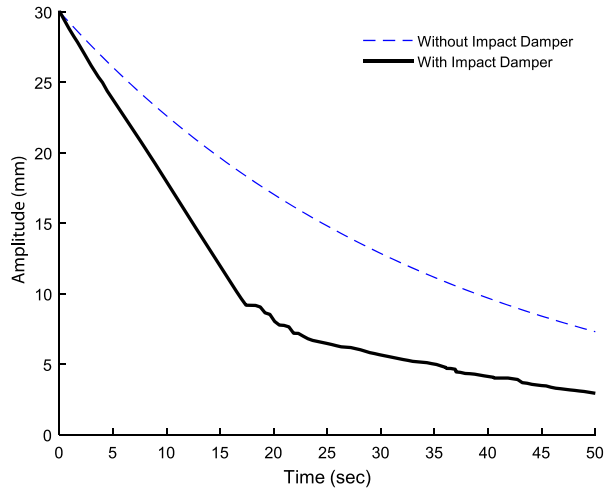
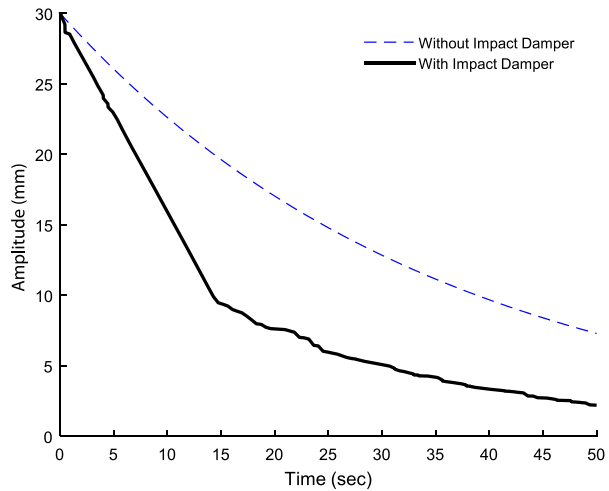


Fig. 17 Amplitude of position of 1-DOF system equipped with impact damper with 50 mm gap size



As shown in these figures, while the gap size increased, the impact damper effect in free vibration reduction improved. When the gap size is very small, the effect of the impact damper is insignificant. For the zero gap size, the impact damper has no effect on the free vibration reduction. In this situation, the system is equivalent to a 1-DOF system without impact damper. When the gap size is very large, greater than twice the initial displacement of 1-DOF system theoretically, the impact mass cannot collide with the end stoppers. Thus the impact damper has no effect on the free vibration reduction. In this situation, the system is equivalent to a 1-DOF system without an impact damper, which is similar to the zero gap size situation.

10 Example 3: a planar slider–crank mechanism

A planar slider–crank mechanism is a classical contact–impact problem in multibody system dynamics. This system consists of five solid bodies representing the slider–crank mechanism

Fig. 18 A slider–crank mechanism and a free sliding block [36]

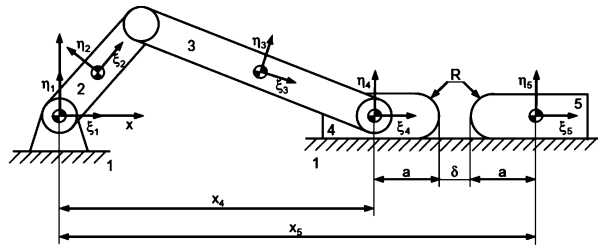


Table 5 Geometrical and inertial properties of multibody system

Body	Length (m)	Mass (kg)	Moments of inertia (kg m ²)
Crank	0.200	0.010	8×10^{-5}
Connecting rod	0.300	0.015	6×10^{-5}
Slider	–	0.050	2×10^{-5}
Free block	–	0.200	3×10^{-5}

Table 6 Initial conditions and simulation configurations of multibody system

Parameter	Value
Initial position of free sliding block	1 m
Initial velocity of free sliding block (to the left)	20 m/s
Angular velocity of rod (counterclockwise)	200 rad/s
The radius of spherical shapes of two contact surfaces	8.5 mm
The contact stiffness parameter of two colliding bodies	9.5×10^9 N/m ^{3/2}
The coefficient of restitution between two colliding bodies	0.7
Distance a	10 mm

and the free sliding block as shown in Fig. 18 [36]. When the slider moves to the right, it collides with the free block and the contact problem occurs. This system represents a multibody model with a total of two degrees of freedom (2-DOF). The geometrical and inertial properties of solid bodies and the initial conditions and simulation configurations of this multibody system are listed in Tables 5 and 6, respectively.

The relative deformation of the slider with respect to the free block can be determined using the following geometrical condition [36]:

$$\delta = x_5 - x_4 - 2a. \tag{70}$$

The crank and the connecting rod are aligned in the x direction at the start of dynamic analysis. Using the constraint equation between the crank and slider, the position and velocity of the slider can be calculated. When the slider and free block collide, the difference in their velocities can be obtained using the new contact force model described in this article.

The time response of positions and velocities of the slider and free block are shown in Figs. 19 and 20, respectively.

At the start of dynamic analysis, the crank rotates counterclockwise and the slider moves to the left. At this time, the free block moves to the left. When time is close to 0.28, the

Fig. 19 The time response of positions of the slider and free block

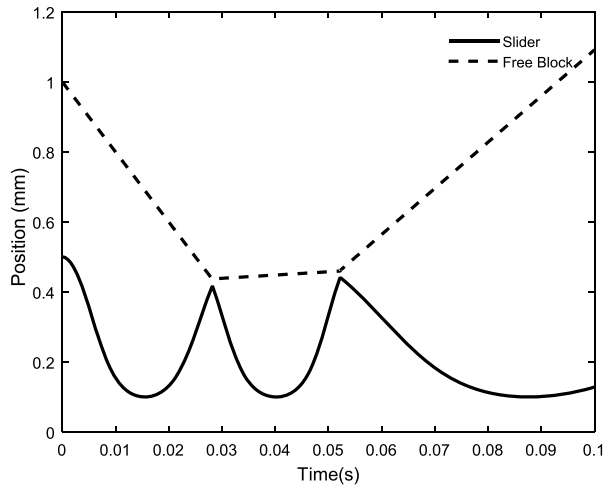
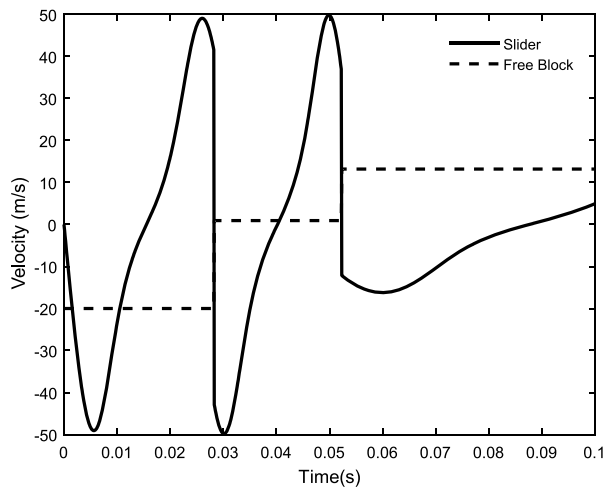


Fig. 20 The time response of velocities of the slider and free block



slider moves to the right and collides with the free block. After collision, the slider moves to the left and the free block moves to the right. As shown in Fig. 19, two collisions between slider and free block occur. After each collision, the velocity of the slider decreased while the velocity of the free block increased.

As shown in this example, the new contact force model described in this article can be used in multibody system dynamics problems.

11 Conclusions

The new model of the contact of the collision between the two solid bodies has been derived in this paper. This model can be used directly for the impact analysis of the multibody dynamics. This model has been developed by using the energy balance during the contact process. The change in the kinetic energy is obtained by using the classical kinetic energy principle. Furthermore, a parametric relation between the deformation and its velocity

is considered. Then the dissipated energy due to the damping force has been calculated. Equating the change in the kinetic energy with the energy loss due to the damping force, an explicit parametric expression between the hysteresis damping factor and the coefficient of restitution is obtained. For determining the unknown constants, the RMS of the percentage error of this expression with respect to the numerical model is minimized. This expression is called the new model which can be used directly for the impact analysis of the multibody dynamic systems.

To sum up, this new model is completely suitable for analyzing the contact process for the whole range of the coefficient of restitution (0–1). So this model is valid for the hard and soft contact problems. Also this model, as an independent formula, can be used directly for impact analysis of the multibody dynamic systems.

Funding This research did not receive any specific grant from funding agencies in the public, commercial, or not-for-profit sector.

Publisher's Note Springer Nature remains neutral with regard to jurisdictional claims in published maps and institutional affiliations.

References

- Varedi, S.M., Daniali, H.M., Dardel, M., Fathi, A.: Optimal dynamic design of a planar slider–crank mechanism with a joint clearance. *Mech. Mach. Theory* **86**, 191–200 (2015). <https://doi.org/10.1016/j.mechmachtheory.2014.12.008>
- Erkaya, S.: Experimental investigation of flexible connection and clearance joint effects on the vibration responses of mechanisms. *Mech. Mach. Theory* **121**, 515–529 (2018). <https://doi.org/10.1016/j.mechmachtheory.2017.11.014>
- Marhefka, D.W., Orin, D.E.: A compliant contact model with nonlinear damping for simulation of robotic systems. *IEEE Trans. Syst. Man Cybern., Part A, Syst. Hum.* **29**(6), 566–572 (1999). <https://doi.org/10.1109/3468.798060>
- Askari, E., Flores, P., Dabirrahmani, D., Appleyard, R.: Study of the friction-induced vibration and contact mechanics of artificial hip joints. *Tribol. Int.* **70**, 1–10 (2014). <https://doi.org/10.1016/j.triboint.2013.09.006>
- Shabana, A.A., Zaazaa, K.E., Escalona, J.L., Sany, J.R.: Development of elastic force model for wheel/rail contact problems. *J. Sound Vib.* **269**(1–2), 295–325 (2004). [https://doi.org/10.1016/S0022-460X\(03\)00074-9](https://doi.org/10.1016/S0022-460X(03)00074-9)
- Afsharfard, A.: Application of nonlinear magnetic vibro-impact vibration suppressor and energy harvester. *Mech. Syst. Signal Process.* **98**, 371–381 (2018). <https://doi.org/10.1016/j.ymssp.2017.05.010>
- Goldsmith, W.: *Impact: The Theory and Physical Behavior of Colliding Solids*. Edward Arnold Ltd., London (1960)
- Hunt, K.H., Crossley, F.R.: Coefficient of restitution interpreted as damping in vibroimpact. *J. Appl. Mech.* **42**(2), 440–445 (1975). <https://doi.org/10.1115/1.3423596>
- Ristow, G.H.: Simulating granular flow with molecular dynamics. *J. Phys. I France* **2**(5), 649–662 (1992). <https://doi.org/10.1051/jp1:1992159>
- Lee, J., Herrmann, H.J.: Angle of repose and angle of marginal stability: molecular dynamics of granular particles. *J. Phys. A, Math. Gen.* **26**(2), 373–383 (1993). <https://doi.org/10.1088/0305-4470/26/2/021>
- Schäfer, J., Dippel, S., Wolf, D.E.: Force schemes in simulations of granular materials. *J. Phys. I France* **6**(1), 5–20 (1996). <https://doi.org/10.1051/jp1:1996129>
- Bordbar, M.H., Hyppänen, T.: Modeling of binary collision between multisize viscoelastic spheres. *J. Numer. Anal. Ind. Appl. Math.* **2**(3–4), 115–128 (2007)
- Zhang, Y., Sharf, I.: Validation of nonlinear viscoelastic contact force models for low speed impact. *J. Appl. Mech.* **76**(5), 051002 (2009). <https://doi.org/10.1115/1.3112739>
- Herbert, R.G., McWhannell, D.C.: Shape and frequency composition of pulses from an impact pair. *J. Eng. Ind.* **99**(3), 513–518 (1977). <https://doi.org/10.1115/1.3439270>
- Gonthier, Y., McPhee, J., Lange, C., Piedboeuf, J.C.: A regularized contact model with asymmetric damping and dwell-time dependent friction. *Multibody Syst. Dyn.* **11**(3), 209–233 (2004). <https://doi.org/10.1023/B:MUBO.0000029392.21648.bc>

16. Zhang, Y., Sharf, I.: Compliant force modeling for impact analysis. In: Proc. The ASME 2004 Design Engineering Technical Conferences and Computers and Information in Engineering Conference, Salt Lake City, Utah, USA, Paper No. DETC2004-57220 (2004)
17. Lee, T.W., Wang, A.C.: On the dynamics of intermittent-motion mechanisms—Part 1: dynamic model and response. *J. Mech. Transm. Autom. Des.* **105**(3), 534–540 (1983). <https://doi.org/10.1115/1.3267392>
18. Kuwabara, G., Kono, K.: Restitution coefficient in a collision between two spheres. *Jpn. J. Appl. Phys.* **26**(8), 1230–1233 (1987). <https://doi.org/10.1143/JJAP.26.1230>
19. Lankarani, H.M., Nikravesh, P.E.: A contact force model with hysteresis damping for impact analysis of multibody systems. *J. Mech. Des.* **112**(3), 369–376 (1990). <https://doi.org/10.1115/1.2912617>
20. Tsuji, Y., Tanaka, T., Ishida, T.: Lagrangian numerical simulation of plug flow of cohesionless particles in a horizontal pipe. *Powder Technol.* **71**(3), 239–250 (1992). [https://doi.org/10.1016/0032-5910\(92\)88030-L](https://doi.org/10.1016/0032-5910(92)88030-L)
21. Brilliantov, N.V., Spahn, F., Hertzsch, J.M., Pöschel, T.: Model for collisions in granular gases. *Phys. Rev. E* **53**(5), 5382–5392 (1996). <https://doi.org/10.1103/PhysRevE.53.5382>
22. Gharib, M., Hurmuzlu, Y.: A new contact force model for low coefficient of restitution impact. *J. Appl. Mech.* **79**(6), 064506 (2012). <https://doi.org/10.1115/1.4006494>
23. Flores, P., Machado, M., Silva, M.T., Martins, J.M.: On the continuous contact force models for soft materials in multibody dynamics. *Multibody Syst. Dyn.* **25**(3), 357–375 (2011). <https://doi.org/10.1007/s11044-010-9237-4>
24. Hu, S., Guo, X.: A dissipative contact force model for impact analysis in multibody dynamics. *Multibody Syst. Dyn.* **35**(2), 131–151 (2015). <https://doi.org/10.1007/s11044-015-9453-z>
25. Flores, P., Lankarani, H.M.: An overview on continuous contact force models for multibody dynamics. In: Proc. The ASME International Design Engineering Technical Conferences & Computers and Information in Engineering Conference IDETC/CIE 2012, Chicago, IL, USA, August 12–15, 2012, Paper No. DETC2012-70393 (2012)
26. Khulief, Y.A.: Modeling of impact in multibody systems: an overview. *J. Comput. Nonlinear Dyn.* **8**(2), 021012 (2013). <https://doi.org/10.1115/1.4006202>
27. Alves, J., Peixinho, N., Silva, M.T., Flores, P., Lankarani, H.M.: A comparative study of the viscoelastic constitutive models for frictionless contact interfaces in solids. *Mech. Mach. Theory* **85**, 172–188 (2015). <https://doi.org/10.1016/j.mechmachtheory.2014.11.020>
28. Flores, P., Lankarani, H.M.: *Contact Force Models for Multibody Systems*. Springer, Switzerland (2016)
29. Skrinjar, P.L., Slavič, J., Boltežar, M.: A review of continuous contact-force models in multibody dynamics. *Int. J. Mech. Sci.* **145**, 171–187 (2018). <https://doi.org/10.1016/j.ijmecsci.2018.07.010>
30. Xiang, D., Shen, Y., Wei, Y., You, M.: A comparative study of the dissipative contact force models for collision under external spring forces. *J. Comput. Nonlinear Dyn.* **13**(10), 101009 (2018). <https://doi.org/10.1115/1.4041031>
31. Johnson, K.L.: *Contact Mechanics*. Cambridge University Press, London (1985)
32. Lankarani, H.M., Nikravesh, P.: Continuous contact force models for impact analysis in multibody systems. *Nonlinear Dyn.* **5**, 193–207 (1994)
33. Big-Alabo, A.: Rigid body motions and local compliance response during impact of two deformable spheres. *Mech. Eng. Res.* **8**(1), 1–15 (2018). <https://doi.org/10.5539/mer.v8n1p1>
34. Meriam, J.L., Kraige, L.G., Bolton, J.N.: *Engineering Mechanics: Dynamics*, 8th edn. John Wiley & Sons, New York (2015)
35. Balachandran, B., Magreb, E.B.: *Vibrations*, 3rd edn. Cambridge University Press, Cambridge (2018)
36. Machado, M., Moreira, P., Flores, P., Lankarani, H.M.: Compliant contact force models in multibody dynamics: evolution of the Hertz contact theory. *Mech. Mach. Theory* **53**, 99–121 (2012). <https://doi.org/10.1016/j.mechmachtheory.2012.02.010>